




Cite this: DOI: 10.1039/d5dt01622c

From discrete to polymeric assemblies: exploring supramolecular structural diversity in transition metal phosphinates with N-donor ligands

Archana Kumari Pattnaik ^{*,a} and Gobinda Chandra Behera^b

A series of coordination complexes derived from diphenylphosphinic acid (DPP) and transition metal ions (Mn(II), Co(II), Ni(II), Cu(II), and Cd(II)) were developed in the presence of various N-donor ligands, including 4,4'-bipyridine (bpy), 1,2-bis(4-pyridyl)ethane (bpvea), 1,2-bis(4-pyridyl)ethene (bpvee), and 1,10-phenanthroline (phen). The resulting structures unveil monomeric, dimeric, and polymeric frameworks, demonstrating the rich structural diversity achievable with phosphinate coordination chemistry. Single-crystal X-ray diffraction analysis revealed variable metal coordination environments—ranging from distorted octahedral to square pyramidal geometries—and highlighted the versatile and intriguing binding modes of DPP, particularly the formation of M–(O–P–O)₂–M eight-membered rings and pseudo-chelating motifs. Notably, rigid co-ligands such as phen result in discrete or dimeric units, while linear spacers like bpy and bpvea facilitate polymeric chain and extended framework development. Solvothermal and ambient crystallisation conditions produced distinct structural outcomes, with cases of polymorphism and framework interconversion observed. Non-covalent interactions, especially hydrogen bonding and π – π stacking, significantly influence the crystal packing pattern and are responsible for the stability of the network solids. These findings highlight the potential of phosphinate-based ligands in constructing coordination networks with tunable dimensionality and topology, thereby expanding the utility of organophosphorus ligands in secondary building unit (SBU) formation and advancing the rational design of supramolecular architectures.

Received 10th July 2025,
Accepted 28th November 2025

DOI: 10.1039/d5dt01622c

rsc.li/dalton

1. Introduction

Organophosphorus acids are an important class of organic substrates for the formation of organic–inorganic hybrid complexes and discrete species to clusters, along with extended networks, showing promising applications in the fields of ion exchange,¹ sorption,^{2–4} catalysts,^{5–7} photoluminescence,⁸ magnetism,^{9,10} *etc.* Organophosphonates, derived from phosphonic acids, show promising applications with variable coordination modes; however, their utility is limited, due to the presence of several strong and potential binding sites that form coordination bonds and non-covalent interactions, leading to the formation of random assemblies rather than targeted structures. However, alkoxy/phenoxy derivatives limit the number of such binding sites to yield targeted ensembles.^{11,12} But, as ester bonds are prone to hydrolysis, the synthetic conditions need to be modulated carefully, such as the pH of the

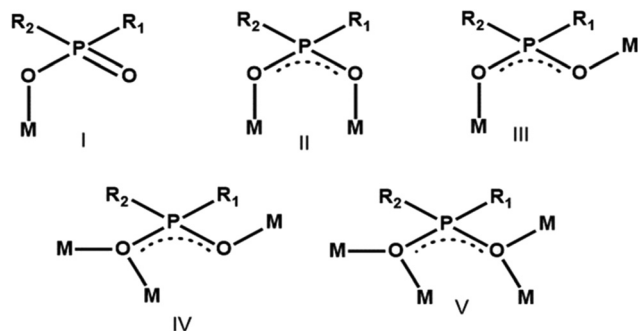
solution, reaction environment, *etc.*, to facilitate complexation without hydrolysis.¹³ Replacing the –OH group with direct P–C bonds—thus avoiding labile alkoxy or phenoxy moieties—enhances the supramolecular features of organophosphorus acids. The resulting phosphines or phosphinites are not only more resistant to hydrolysis, but their tunable functional groups also allow precise control over binding sites, enabling the formation of tailored hybrid structures under more flexible reaction conditions.^{14,15} This strategy opens up adequate ways to achieve complexes with active metal sites within the framework to exhibit substantial applications.¹⁶ In fact, diaryl and dialkyl phosphinic acids represent a relatively small fraction of known MOF structures compared to carboxylates, although they readily form coordination complexes through diverse metal–oxygen binding modes, typically resulting in non-porous and layered architectures.¹⁴ Among the possible coordination modes (Scheme 1), the common mode seen in phosphinate complexes is II (Scheme 1), which generally forms an 8-membered ring (M–O–P–O–M–O–P–O), as also noted in phosphates and phosphonates.

Apart from these modes of coordination, pseudo-chelation is also observed in many heteroleptic complexes, due to strong H-bond donors/acceptors in the ligands. When both phosphi-

^aSupramolecular and Solid State Structural Chemistry Laboratory, School of Basic Sciences, Indian Institute of Technology Bhubaneswar, Bhubaneswar 752 050, India. E-mail: akp18@iitbbs.ac.in, arcpattnaik@gmail.com

^bDepartment of Chemistry, Maharaja Purna Chandra Autonomous College, Takhatpur, Baripada 757003, Odisha, India





Scheme 1

nates and phosphinic acids are coordinated to a single metal atom, then pseudo-chelation ($\text{O}-\text{PR}_2=\text{O}\cdots\text{H}-\text{O}-\text{PR}_2=\text{O}$) is established. These distinctive features, indeed, exhibit a significant role in the metal extraction process mechanism using phosphinate ligands (Fig. 1).^{17,18}

From a CSD search, it is apparent that among the eighteen possible modes, the most common binding mode is the dinucleating form 2.11 (Harris notation for mode II in Scheme 1), which is frequently observed in discrete, oligomeric and polymeric structures reported. For example, $[\text{Ni}_2(\mu_2\text{-L1})_2(2,2'\text{-dipy})_4]^{2+}$ and $[(\text{py})_3\text{Co}_2(\mu_2\text{-L2})_3\text{py}]^+$ are two complexes as illustrated in Fig. 2, in which the phosphinate group ($\text{O}-\text{P}-\text{O}$) bridges metal atoms.^{20,21} The Ni complex [Fig. 2(a)] which contains $-\text{PH}$ group as a bridging unit, is of high significance because it enables direct functionalisation to tailor the structure and the properties of materials, such as catalysts and magnetoactive systems.²² $\text{Ni}-(\text{O}-\text{P}-\text{O})_2\text{-Ni}$ with the eight membered heterocycle in a chair form involves a distorted octahedral environment around $\text{Ni}(\text{II})$, with a *cis* arrangement of oxygen atoms [Fig. 2(a)]. However, the complex shown in Fig. 2(b) is a dinuclear complex with mixed geometry of cobalt (both octahedral and tetrahedral sites), with the dibenzyl phos-

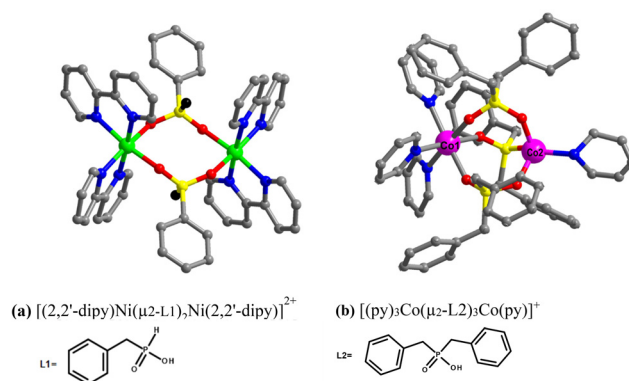


Fig. 2 Examples of dinuclear structures containing (a) two and (b) three bridging motifs (see Scheme 1(II)).

phinate ligand bridging the metal nodes, showing antiferromagnetic activity.

Apart from this, these versatile phosphinate ligands also form linear polymeric chains bridging metal ions and show trinucleating,^{23,24} tetranucleating,²⁵ and pentanucleating^{26–28} motifs through different coordination modes (Scheme 1). Similarly, polyphosphinic acids with non-chelating auxiliary ligands like bpy and its derivatives generate *polymeric* complexes with 2D and 3D frameworks acquiring permanent porosity. In fact, by using these strategies, a series of MOFs (ICR 2, 4, 6 and 7) have been reported in the literature.²⁸ As the most common bridging is bidentate bridging, the obtained geometry, in general, is 1D polymeric chains, which show magnetic activity. Also, it is observed that phosphinates have more propensity for the formation of a large number of high-density polynuclear clusters than MOFs. In this study, we have used diphenyl phosphinic acid as a phosphorus containing ligand along with different N-donor coligands, incorporating transition metal ions to investigate herein the interactions of ligands with metal ions. Thus, the intriguing structural landscape with diverse architectures depends on novel arrangements and directions of building blocks to form discrete, polymeric and cluster structures that disperse ligand coordination features.

Possible coordination modes (Scheme 1) of phosphinic acids are able to develop interesting building blocks for coordination complex assemblage, as their coordination modes are similar to those of widely studied carboxylates, but their complexation process follows a distinct way. According to the HSAB principle, the acidity of phosphinic acids also falls between those of carboxylic and phosphonic acids.

To achieve the higher dimensionality of the polymer network containing metal phosphinates, auxiliary ligands also play a pivotal role, which ultimately influence the topology and the physico-chemical behaviour of the complexes. Therefore, diphenylphosphinic acid (**DPP**), which is a monophosphinic acid along with different N-donor compounds such as 4,4'-bipyridine (bpy), 1,2-bis(4-pyridyl)ethane (bpvea), 1,2-bis(4-pyridyl)ethene (bpvee) and 1,10-phenanthroline (110phen), in

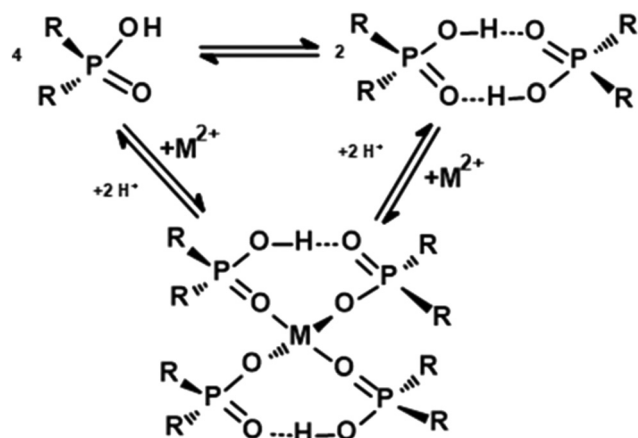
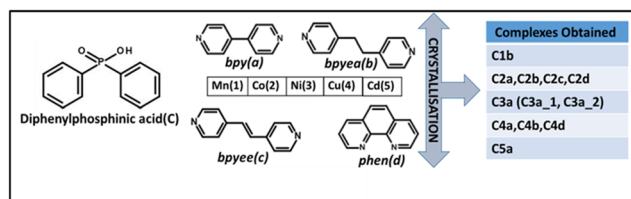


Fig. 1 Monomeric and dimeric forms of phosphinic acid showing retention of interligand H-bonding upon the formation of a tetrahedral complex.¹⁹





Scheme 2

the presence of transition metal species (Mn(II), Co(II), Ni(II), Cu(II) and Cd(II)) is crystallised, as listed in Scheme 2 through various crystallisation procedures. The structural features in terms of bonding and spatial arrangement of molecules in the lattice for the crystals obtained as listed in Scheme 2 are discussed in the following sections.

2. Experimental section

All reagents (metal salts – Mn(NO₃)₂·4H₂O, Co(NO₃)₂·6H₂O, Ni(NO₃)₂·6H₂O, Cu(ClO₄)₂·6H₂O and Cd(NO₃)₂·6H₂O) and organic ligands – diphenyl phosphinic acid (DPP), 4,4'-bipyridine (bpy), 1,2-bis(4-pyridyl)ethane (bpyea), 1,2-bis(4-pyridyl)ethene (bpyee) and 1,10-phenanthroline (110phen) of utmost purity – were purchased from commercial suppliers and used without any further purification. For the crystallisation experiments, spectroscopy-grade solvents and distilled water were used.

2.1. Preparation of molecular complexes

All complexes were prepared by dissolving DPP (0.05 mmol) in 3 mL of CH₃OH by gentle heating on a water bath and adding an aqueous solution of the corresponding metal ion (0.1 mmol in 2 mL of H₂O), followed by dropwise addition of methanolic solution of ligands (a–d) (0.05 mmol in 2 mL of CH₃OH), thus maintaining a molar ratio for DPP:metal salt:N-donor ligands of 1:2:1 in all complexes. The reaction mixture was allowed to slowly evaporate at room temperature to afford the crystals of C2d, C3a_1, and C5a. Within 24–72 h, crystals appeared in the solution. All other complexes except C4a were crystallised using a solvothermal method, keeping the reaction mixture solution in a 25 mL Teflon vessel inside a stainless steel chamber maintained at 130 °C for two days, followed by cooling at a rate of 5 °C h^{−1}. After that, the solution was allowed to slowly evaporate at room temperature. The C4a reaction mixture solution was kept in a vacuum for crystallisation through vacuum evaporation. In these processes, crystals appeared within a week, which were separated for the characterization using the X-ray diffraction technique.

2.2. Characterization

2.2.1. Single crystal X-ray structure determination. Good quality single crystals of all complexes were chosen with the help of a Leica Stereo Zoom microscope and mounted using a loop with Paratone-N on the goniometer of a Bruker Single

Crystal X-ray diffractometer (D8 VENTURE) equipped with a PHOTON 100 CMOS detector and microfocus Mo-Kα radiation ($\lambda = 0.71073$ Å). The crystals were stable and data collection was smooth without any complications. Single-crystal X-ray diffraction data were collected for the complexes at different temperatures depending on the crystal quality: for some structures, measurements were carried out under ambient conditions (293 K), while for others, data were collected at a low temperature (100 K) to improve diffraction quality. The crystal structures were solved by the intrinsic phasing method and refined using full-matrix least-squares procedures against F^2 with SHELXTL. All non-hydrogen atoms were refined anisotropically, while hydrogen atoms were either located from difference Fourier maps or placed in geometrically calculated positions and refined using a riding model. The obtained three-dimensional structures of the complexes, in the form of ORTEP, are given in the SI. All intermolecular interactions were computed by using PLATON software and packing diagrams were generated using Diamond (version 4.6.8). All H atoms, including those on coordinated/lattice water molecules, were included in the refinement model. Water H atoms were located from difference maps and refined with restrained geometry. For clarity, hydrogen atoms are omitted from the structural drawings/packing diagrams.

3. Results and discussion

3.1. Structural description of the metal phosphinate ensembles

3.1.1. Structural arrangement in Mn(II) complex with DPP and bpyea. Crystallization of Mn(CH₃COO)₂·4H₂O in the presence of DPP with N-donor ligands, listed in Scheme 1, from a solution of MeOH–H₂O, forms corresponding single crystals suitable for structure determination by X-ray diffraction, except with 110phen. The complexes with bpy and bpyee (C1a and C1c, respectively) correspond to the structures already reported in the literature,²⁹ which form 1D polymer chains containing DPP, and tetraphenylimidodiphosphinates along with Mn(II) and bpy or bpyee, as the case may be. However, C1b: C₃₆H₃₂N₂O₄P₂Mn (DPP, Mn(II) and bpyea) crystallises in a monoclinic space group, $P2_1/n$, which contains Mn(II) in an octahedral core, coordinating with four DPP and two bpyea molecules. C1b ($P2_1/n$, $Z = 2$) Mn1 lies on an inversion centre at (0.5, 0, 0.5) (ASU occupancy 0.5, tied to fvar(1)) and is coordinated by N1 of a symmetry-related half bpyea ligand and O1 of a DPP ligand; the complete complex is generated by inversion symmetry. Contents of asymmetric units in the form of ORTEP at 50% probability are given in the SI. The pertinent crystallographic parameters are listed in Table 1.

In such coordination bonding, Mn–N distances lie in the range of 2.141–2.171 Å and the Mn–O distance is 2.331 Å. The pertinent bond characteristics are listed in Table 2. In particular, the bonding pattern between DPP and Mn(II) is in the most common bidentate bridging form, mode II (Scheme 1), thus yielding a M–(O–P–O)₂–M ring motif. Packing analysis of





Table 1 Crystallographic information of the complexes (C1b, C2a–C2d, C3a_1, C3a_2, C4a, C4b, C4d and C5a)

	C1b	C2a	C2b	C2c	C2d
Formula	C ₃₆ H ₃₂ N ₂ O ₄ P ₂ Mn	C ₃₄ H ₃₄ N ₂ O ₇ P ₂ Co	C ₃₆ H ₃₄ N ₂ O ₅ P ₂ Co	C ₈₄ H ₆₈ N ₆ O ₂₂ P ₄ Co ₂	C ₄₈ H ₃₆ N ₆ O ₁₀ P ₂ Co ₂
<i>F</i> _w	673.51	703.50	695.52	1785.42	1036.63
Crystal colour	Colourless	Pink	Pink	Pink	Pink
Crystal shape	Plate	Plate	Block	Block	Block
<i>T</i> /K	293(2)	100(2)	293(2)	100(2)	100(2)
Mo <i>k</i> _α /Å	0.71073	0.71073	0.71073	0.71073	0.71073
Crystal system	Monoclinic	Monoclinic	Triclinic	Triclinic	Monoclinic
Space group	<i>P</i> ₂ / <i>1</i> / <i>n</i>	<i>P</i> ₂ / <i>1</i> / <i>c</i>	<i>P</i> $\bar{1}$	<i>P</i> $\bar{1}$	<i>P</i> ₂ / <i>1</i> / <i>n</i>
<i>a</i> /Å	13.7783(14)	11.4798(13)	11.9816(17)	13.5255(16)	12.5496(15)
<i>b</i> /Å	5.6132(7)	27.409(4)	12.7736(17)	13.5524(15)	12.9240(17)
<i>c</i> /Å	20.880(3)	11.5762(14)	13.4767(17)	14.8154(16)	14.449(2)
<i>a</i> /°	90	90	112.507(4)	98.577(4)	90
<i>β</i> /°	94.922(3)	119.306(4)	91.947(5)	104.184(4)	104.083(4)
<i>γ</i> /°	90	90	115.772(4)	119.379(3)	90
<i>V</i> /Å ³	1608.9(3)	3176.3(7)	1665.4(4)	2174.6(4)	2273.1(5)
<i>Z</i>	2	4	2	1	2
<i>D</i> _c /g cm ^{−3}	1.390	1.471	1.387	1.363	1.515
<i>μ</i> /mm ^{−1}	0.552	0.694	0.657	0.530	0.867
<i>F</i> (000)	698	1460	722	934	1060
Crystal size/mm ³	0.32 × 0.25 × 0.20	0.29 × 0.23 × 0.18	0.32 × 0.23 × 0.12	0.25 × 0.11 × 0.11	0.29 × 0.20 × 0.15
2 θ _{max}	56.76	56.786	56.864	57.024	56.99
Total reflections	25 972	59 751	34 937	32 061	36 889
Unique reflections	4002	7896	8282	10 882	5718
Completeness (%)	99.3%	99.8%	99.9%	99.0%	99.7%
No. of parameters	205	433	421	577	307
Goodness-of-fit on <i>R</i> ²	1.038	1.112	1.021	1.025	1.054
<i>R</i> ₁ [<i>I</i> > 2 σ]	0.0328	0.0500	0.0434	0.0340	0.0393
<i>wR</i> ₂ [<i>I</i> > 2 σ]	0.0944	0.0966	0.1053	0.0943	0.1023
CCDC number	2290893	2290901	2290894	2290898	2290896

	C3a_1	C3a_2	C4a	C4b	C4d	C5a
Formula	C ₃₄ H ₃₂ N ₂ O ₆ P ₂ Ni	C ₄₄ H ₄₀ N ₅ O ₁₂ P ₂ Ni	C ₃₄ H ₂₉ ClN ₂ O ₉ P ₂ Cu ₂	C ₂₄ H ₂₂ ClN ₂ O ₆ PCu	C ₂₄ H ₂₀ ClN ₂ O ₇ PCu	C ₄₆ H ₃₈ N ₂ O ₈ P ₃ Cd
<i>F</i> _w	685.26	958.51	834.06	564.39	578.38	920.09
Crystal colour	Pale green	Pale green	Blue	Blue	Blue	Colourless
Crystal shape	Rod	Block	Rod	Rod	Rod	Block
<i>T</i> /K	293(2)	100(2)	293(2)	293(2)	293(2)	293(2)
Mo <i>k</i> _α /Å	0.71073	0.71073	0.71073	0.71073	0.71073	0.71073
Crystal system	Monoclinic	Tetragonal	Monoclinic	Monoclinic	Orthorhombic	Monoclinic
Space group	<i>C</i> ₂ / <i>c</i>	<i>P</i> ₄ ₃ ₂ ₂	<i>C</i> ₂ / <i>c</i>	<i>P</i> ₂ / <i>1</i> / <i>c</i>	<i>P</i> <i>bca</i>	<i>C</i> ₂ / <i>c</i>
<i>a</i> /Å	26.447(5)	11.3016(11)	25.424(3)	13.2632(14)	21.733(3)	22.865(2)
<i>b</i> /Å	11.211(2)	11.3016(11)	11.3058(14)	16.5624(18)	9.2303(10)	11.7446(8)
<i>c</i> /Å	11.2987(16)	33.869(5)	25.572(3)	11.6242(12)	23.419(3)	32.081(2)
<i>a</i> /°	90	90	90	90	90	90
<i>β</i> /°	92.771(9)	90	113.557(4)	104.254(3)	90	100.258(4)
<i>γ</i> /°	90	90	90	90	90	90
<i>V</i> /Å ³	3346.0(10)	4325.9(11)	6737.8(14)	2474.9(5)	4697.8(10)	8477.1(11)
<i>Z</i>	4	4	8	4	8	8
<i>D</i> _c /g cm ^{−3}	1.360	1.472	1.644	1.515	1.636	1.442
<i>μ</i> /mm ^{−1}	0.721	0.593	1.496	1.098	1.162	0.679
<i>F</i> (000)	1424	2000	3392	1156	2360	3752

Table 1 (Contd.)

	C3a_1	C3a_2	C4a	C4b	C4d	C5a
Crystal size/mm ³	0.35 × 0.31 × 0.21	0.31 × 0.23 × 0.19	0.25 × 0.20 × 0.14	0.33 × 0.25 × 0.20	0.25 × 0.2 × 0.12	0.35 × 0.23 × 0.11
$2\theta_{\max}$	56.806	56.768	57.512	57.068	56.982	56.558
Total reflections	27 581	86 218	56 626	38 255	75 215	43 929
Unique reflections	4174	5419	8575	6227	5928	10 488
Completeness (%)	99.8%	99.6%	99.9%	99.9%	99.9%	99.9%
No. of parameters	212	311	455	316	331	523
Goodness-of-fit on R^2	1.039	1.044	1.036	1.036	1.060	0.993
R_1 , [$I > 2\sigma$]	0.0390	0.0462	0.0335	0.0443	0.0370	0.0428
wR_2 , [$I > 2\sigma$]	0.0974	0.1142	0.0793	0.1129	0.0903	0.1197
CCDC number	2290897	2290903	2290902	2290895	2290900	2290899

Table 2 Bond distances (Å) of the coordination environment and P–O in DPP (esds are shown in parentheses)

Complex	M–O	M–N	P–O
C1b	2.141(1) 2.171(1)	2.331(1)	1.493(1) 1.502(1)
C2a	2.051(2) 2.056(2) 2.130(2) 2.183(3)	2.159(3) 2.205(3)	1.507(2) 1.510(3) 1.511(3) 1.515(3)
C2b	2.056(1) 2.059(1) 2.097(1) 2.197(1)	2.148(2) 2.152(2)	1.482(1) 1.492(1) 1.498(1) 1.501(1)
C2c	2.094(1) 2.104(1) 2.121(1) 2.129(1)	2.107(1) 2.166(1)	1.505(1) 1.506(1) 1.515(1)
C2d	1.997(1) 2.005(1) 2.154(1) 2.267(1)	2.119(2) 2.122(2)	1.489(1) 1.501(1)
C3a_1	2.060(1) 2.124(1)	2.086(3) 2.095(2)	1.498(2) 1.499(2)
C3a_2	2.089(5) 2.095(5)	2.107(4) 2.110(4) 2.115(4) 2.124(4)	1.501(5) 1.508(5) 1.550(5) 1.551(5)
C4a	1.924(1) 1.939(1) 1.962(1) 1.963(1) 1.984(1) 2.029(1) 2.320(1) 2.339(1)	2.013(1) 2.016(1)	1.504(1) 1.509(1) 1.512(1) 1.519(1)
C4b	1.929(1) 1.934(1) 2.561(1)	1.995(2) 2.004(2)	1.509(1) 1.511(1)
C4d	1.939(1) 1.955(2) 2.325(2)	1.997(2) 2.009(2)	1.498(1) 1.514(1)
C5a	2.250(2) 2.274(3) 2.275(2) 2.276(2)	2.365(3) 2.377(3)	1.487(3) 1.495(3) 1.523(3) 1.535(3)

molecules in **C1b** reveals that the coordination moieties also form polymeric chains, as observed in **C1a** and **C1c** (reported in the literature). In the three-dimensional arrangement, the units in **C1b** are held together by C–H... π interactions as denoted in Fig. 3, representing an arrangement of polymeric chains, stabilized by appropriate metal–organic bonds (Mn–O and Mn–N). Apart from two weak intermolecular C–H...O contacts ($D\cdots A = 3.620$ and 3.954 Å), no other significant hydrogen-bonding interactions are present; the packing is thus dominated by van der Waals contacts (see SI(II)).

3.2. Structural description of Co(n) complexes (C2a–C2d)

DPP, along with metal ion species Co(n), successfully forms complexes, **C2a–C2d**, with N-donors, as listed in Scheme 2. These complexes show some similarities despite each one showing its specific molecular arrangement. All complexes contain the metal ion Co(n), in a distorted octahedral geometry by coordinating with four oxygen atoms and two nitrogen



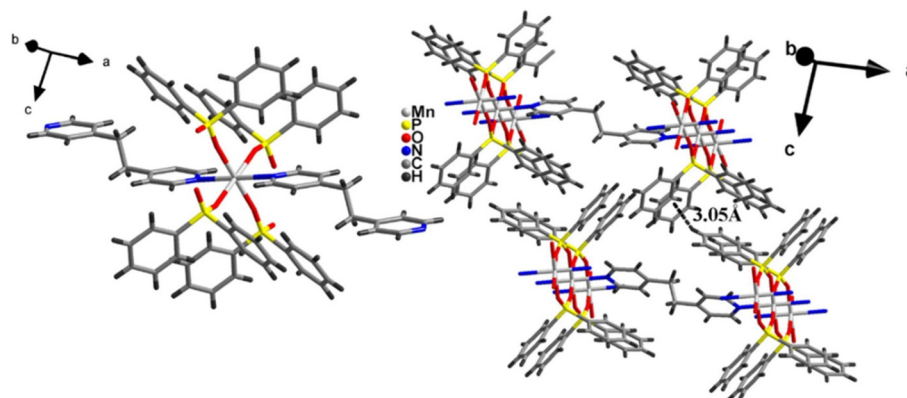


Fig. 3 Coordination fragment of **C1b** (left). Packing diagram showing C–H... π interaction (right).

atoms, which are from organic ligands and solvent molecules. Among the structures, **C2a**: $\text{C}_{34}\text{H}_{34}\text{N}_2\text{O}_7\text{P}_2\text{Co}$ and **C2d**: $\text{C}_{48}\text{H}_{36}\text{N}_6\text{O}_{10}\text{P}_2\text{Co}_2$ crystallise in the monoclinic space groups $P2_1/c$ and $P2_1/n$ respectively, whereas **C2b**: $\text{C}_{36}\text{H}_{34}\text{N}_2\text{O}_5\text{P}_2\text{Co}$ and **C2c**: $\text{C}_{84}\text{H}_{98}\text{N}_6\text{O}_{22}\text{P}_4\text{Co}_2$ crystallise in the triclinic space group, $P\bar{1}$. The complete structure determination parameters are listed in Table 1. The asymmetric unit contents in each complex are presented in the SI. Thus, apart from coordination spheres, in crystals of **C2a** and **C2c**, uncoordinated water molecules are also present, while in the **C2d** counter anion, nitrate is also present in the asymmetric unit, coordinating to Co(II), apart from the other bonding features mentioned above. Furthermore, interestingly, the coordination of solvent molecules (H_2O), indeed, leads to a pseudo-chelation form, instead of metal phosphinate 8-membered ring formation *via* bidentate bridging of **DPP**, in some complexes. Furthermore, in the structure of **C2c**, surprisingly, **DPP** molecules lie in the asymmetric unit without coordinating to Co(II) at all. Complete details of each complex with pertinent details of interactions between molecules, bonding patterns, coordination features, etc., are discussed below.

In **C2a**, as shown in Fig. 4, two bpy and **DPP** molecules along with a similar number of water molecules coordinate to Co(II). Co1 (general position) binds two DPP O atoms, O3/O5

(H_2O), and N1(bpy); the sixth site is occupied by N2(phen) from a symmetry mate at $1 + x, y, z$. Apart from this, lattice water O7 also occupies a general position as shown in the ORTEP (SI). All H atoms—including those on O3, O5 and O7—are sensibly located and refined. In such bonding, the observed Co–O and Co–N distances are in the ranges of 2.051–2.183 Å and 2.159–2.205 Å, respectively. Complete details of the bonding parameters are given in Table 2. The coordination spheres further extend through bpy molecules bridging adjacent metal centres, in the form of a 1D polymeric structure.

In two-dimensional assembly, the adjacent chains while interact with each other through C–H...O hydrogen bonds, with a H...O distance of 2.47 Å, formed between coordinated water (O) and bpy (–CH) molecules. In addition, the occluded water molecules between the chains also interact through similar interactions but with a H...O distance of 2.51 Å. Besides, though **DPP** possesses bidentate features, in complex **C2a**, the coordination reflects a monodentate feature, ensuring O–H...O (O...O, 2.673 and 2.778 Å) and C–H...O (H...O, 2.73 Å) hydrogen bonds with water molecules by connecting primary coordination spheres (inset in Fig. 5). Besides these, lattice water molecules (O7W) are also attributed to strong O...O interactions, as shown in Fig. 5.

Complex **C2b** upon structure determination by X-ray diffraction reveals that in its crystal lattice, the asymmetric unit shows a Co(II) ion along with three **DPP** and two bpypa molecules as well as a water molecule. The asymmetric unit as shown in ORTEP (see the SI(I)) has Co1 in a general position directly bonded to N1 of a (bpypa) ligand, to O2 and O4 of two DPP ligands, and to water oxygen O3. The Co1 coordination is completed by a bond to N2 of the (bpypa) ligand at $(x, y, -1 + z)$. All H atoms including those on the water molecule O3 appear to be correctly placed. The salient crystallographic data are listed in Table 1.

The observed coordination bonds are in the ranges of 2.056–2.197 Å and 2.148–2.152 Å, respectively. In this process, each Co(II) center exists in an octahedral geometry (see Fig. 6). The coordination bond features are listed in Table 2. Furthermore, such coordination spheres extend into a polymeric form (see Fig. 7).

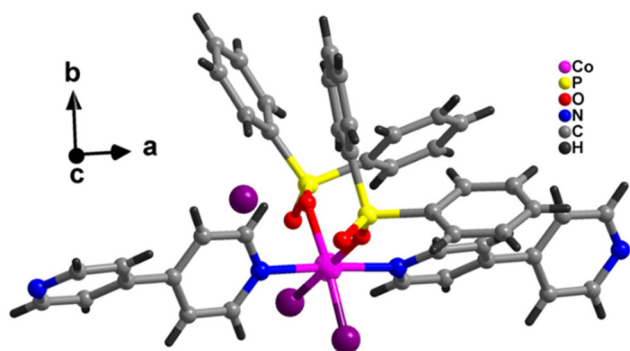


Fig. 4 Coordination sphere of **C2a**, with two water molecules coordinating and one in the lattice site (oxygen atom in purple).



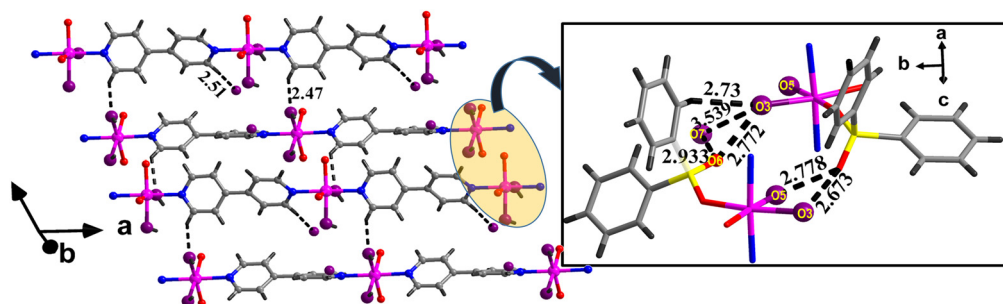


Fig. 5 Packing diagram of **C2a**; phenyl rings are omitted from **DPP** for clarity and water molecules are presented in purple (left). Pseudo-chelation through H-bonding (right).

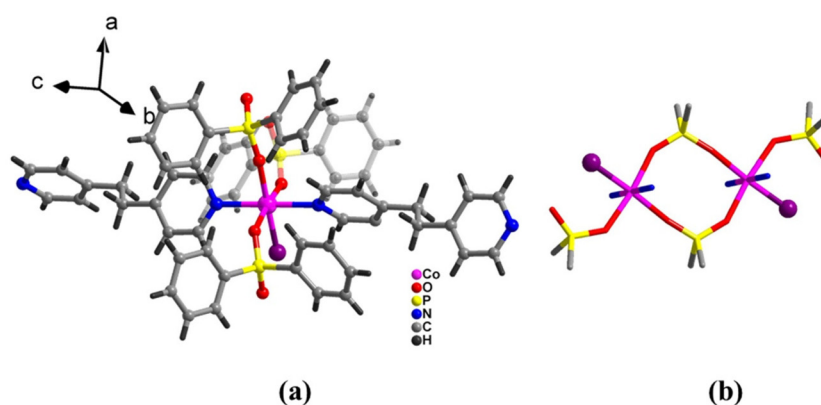


Fig. 6 (a) Octahedral coordination sphere of **C2b**, with one-water molecule coordinating (oxygen atom in purple). (b) Dimeric complex of **C2b**.

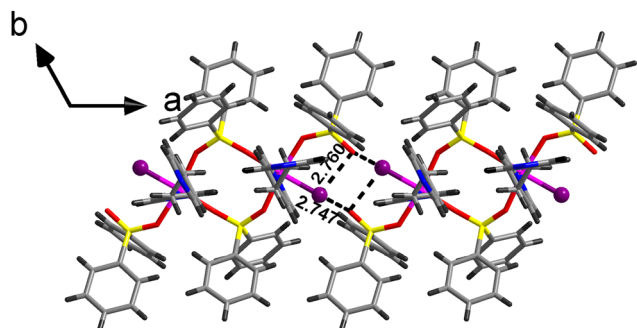


Fig. 7 2D packing diagram of **C2b** with the O...O distance shown in Å.

Among three **DPP** ligands, two follow bidentate bridging, as shown in Fig. 6(b) in the form of a typical 8-membered ring, involving the M-(O-P-O)₂-M moiety. The remaining **DPP** molecule also indeed forms a similar (pseudo) chelating bonding pattern, with the aid of hydrogen bonds along with coordination bonds (Fig. 7). The hydrogen bonds [O...O, 2.747 Å (intermolecular) and 2.760 Å (intramolecular)], that constitute this motif are annotated in Fig. 7, where the corresponding hetero atom distances are indicated. Thus, herein, the flexibility of phosphinate ligands further demonstrates the

efficacy of H-bonds in accordance with coordination bonds, towards establishing specific topological arrangements.

In coordination polymers, **C2c**, **DPP** and Co(II), in the presence of a linear spacer, bpyee, under solvothermal conditions, crystallise as rod like crystals, in the triclinic $P\bar{1}$ space group. Complete crystallographic parameters are given in Table 1 and the ORTEP is illustrated in SI(I). The asymmetric unit has two Co atoms, Co1 and Co2, lying on inversion centres. The half-occupancy Co1 atom is directly bonded to N2 of a complete bpyee ligand and to two water oxygens O1 and O2. The half-occupancy Co2 atom is directly bonded to two water oxygens O3 and O4 and to the N1 atom of half of a bpyee ligand, which lies about another inversion centre. There are also three water molecules, O9, O10, and O11, in general positions in lattice sites. All H atoms, including those on the water oxygen atoms, appear to be correctly placed. Thus, in the crystal lattice, apart from coordinated motifs, two uncoordinated molecules of **DPP** and three molecules of water are also present. In crystals **C2c**, Co(II) forms two different coordination environments, labelled as A and B, as shown in Fig. 8, with the environments shown in different colors (A in grey and B in yellow). In both the environments, Co(II) is present in an octahedral geometry, with the coordination of two bpyee and four water molecules, with the corresponding Co-O and Co-N distances in the ranges of 2.094–2.129 Å and 2.107–2.166 Å, respectively.



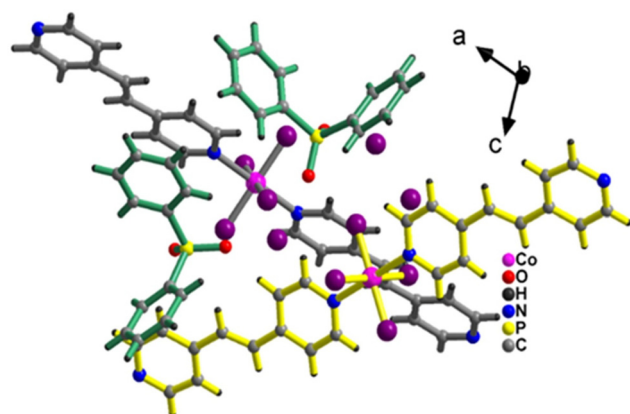


Fig. 8 Two independent units present in C2c illustrated in grey colour bonds and yellow colour bonds along with coordinated/uncoordinated water molecules (purple) and DPP molecules (green colour bonds).

In the crystal lattice, the two independent coordination units, A and B, aggregate through O–H...O, O–H...N and C–H...O hydrogen bonds. All hydrogen bond parameters are listed in SI(II). The corresponding H...O (O–H...O) distances lie in the range from 1.66 to 1.91 Å, whereas H...O (C–H...O) distances are observed to be between 2.37 and 2.55 Å. O11–H11A...N3 with a H...N distance of 1.78 Å is also attributed to the consolidated packing of the coordination assembly (see Fig. 9). Furthermore, the coordination sphere A polymer is found to be a linear chain extended to a polymeric form through the N-terminal of bpyee ligands coordinating with Co (II), while B is a discrete unit arranged in such a manner that it forms a host-kind of assemblage such that unit A is fit within the voids thus created. The arrangement of such a topology is shown in Fig. 9. Thus, it is clearly reflective that unlike in C2a

and C2b, DPP molecules do not form coordination bonds with Co(II) and only participate in the creation and stabilization of secondary spheres.

Coordination assembly of C2d is obtained upon crystallization of $\text{Co}(\text{NO}_3)_2 \cdot 6\text{H}_2\text{O}$ in the presence of DPP along with the rigid linker 110phen by slow evaporation of a CH_3OH solution, under ambient conditions. A peculiar observation during the formation of crystals is that block shaped crystals were obtained at the neck of the conical flask rather than in the bulk of the solution. Structure determination by X-ray diffraction reveals that the asymmetric unit consists of a nitrate anion (counter ion in the metal salt) along with other organic ligands and Co(II). C2d crystallizes in a monoclinic space group, $P2_1/n$. Structure determination parameters are listed in Table 1 and contents of the asymmetric unit (ORTEP) are presented in SI(I). Co(II) is coordinated with DPP and 110phen molecules and also the nitrate anion. Another interesting feature in the coordination aspects is that the coordination sphere remains in the form of discrete units as 110phen molecules do not modulate the propagation and in fact, it binds to Co(II) in a bidentate mode with Co–N distances being 2.119 and 2.122 Å. Also, the coordinated nitrate anion does not facilitate the realization of an infinite network in any direction, due to its bidentate mode of bonding. With such a coordination network around Co(II), it forms an octahedral geometry. Thus, the molecule is a centrosymmetric dimer; Co1 (general) binds N2/N3(phen), O3/O5 (NO_2), and O2(DPP), with the sixth site occupied by O1 from the inversion-related position at $(1-x, 1-y, 1-z)$.

The nitrate ion, however, participates in noncovalent interactions (C–H...O hydrogen bonds) connecting adjacent coordinated fragments, as shown in the inset of Fig. 11. Such interactions are through both DPP (H...O, 2.19 Å) and 110phen (H...O, 2.29 and 2.58 Å). In addition, 110phen ligands present

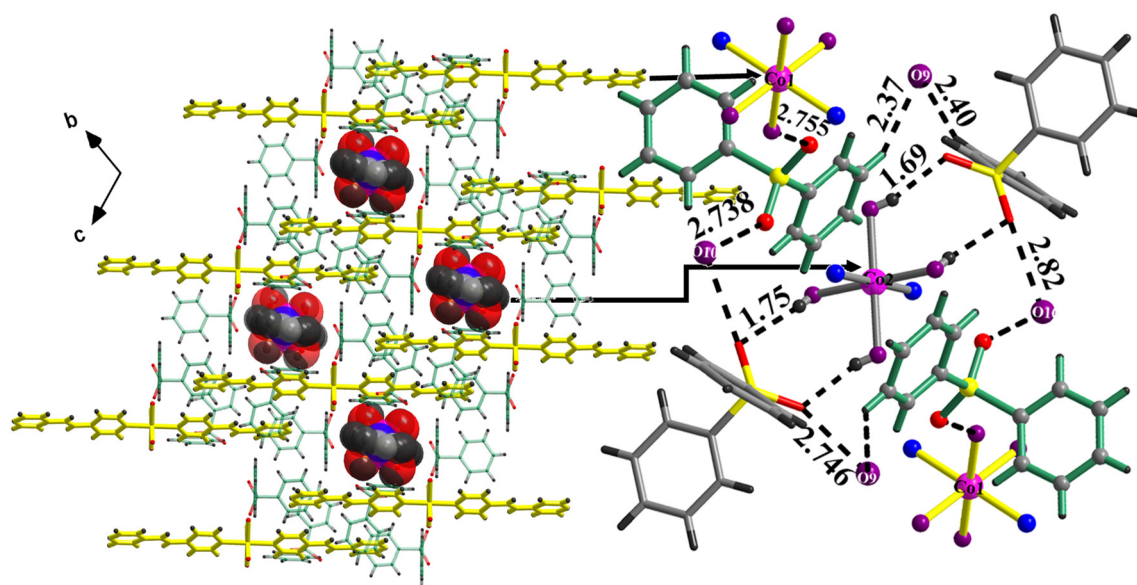


Fig. 9 Grid arrangement of A and B in C2c with a host–guest topology (left) and enlarged picture showing the O–H...O bonds between coordinated and uncoordinated motifs (right).



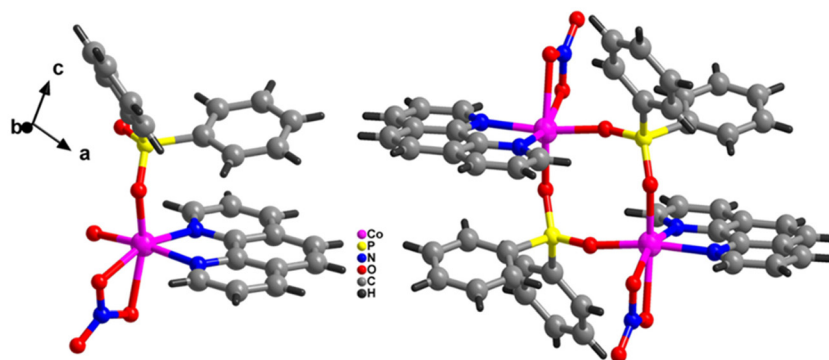


Fig. 10 Asymmetric unit of C2d illustrating the chelated coordination environment (left) and the dimeric complex (right).

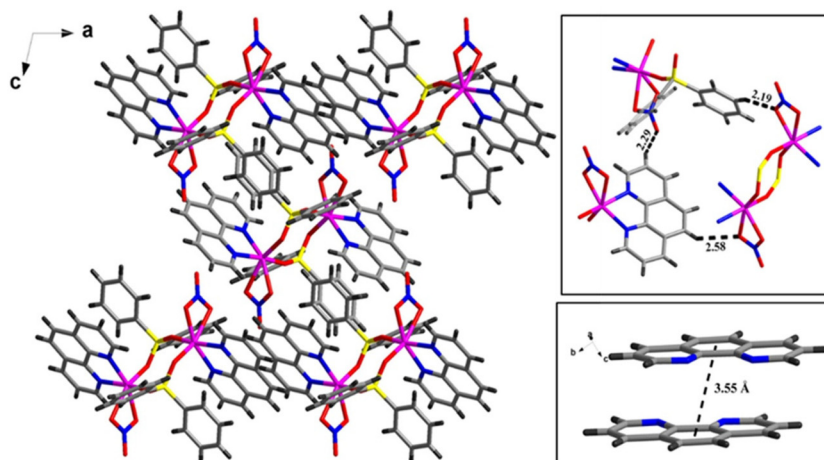


Fig. 11 2D packing arrangement of fragments in the crystal lattice of C2d. C–H...O and π – π interaction distances are shown in the inset.

in adjacent coordinated fragments contribute to structure stabilization through π – π interaction (3.55 Å). Such interactions are presented in the inset of Fig. 11 and other hydrogen bond parameters are listed in SI(II).

3.3. Structural elucidation of Ni(II) complexes, C3a_1 and C3a_2, with DPP in association with 4,4'-bipyridine (bpy)

Ni(II) nitrate along with DPP and bpy upon crystallisation forms different types of crystals, depending upon the methods followed and also the solvent employed in the crystallization process, although the same molecular composition is maintained. The crystals obtained from a slow evaporation of a CH₃OH solution are labelled as C3a_1 (C₃₄H₃₂N₂O₆P₂Ni), while the crystals obtained from a solvothermal process are labelled as C3a_2 (C₄₄H₄₇N₅O₁₂P₂Ni). The solvothermal process involves keeping the solution in a Teflon container inside the stainless steel chamber maintained at 130 °C for three days followed by cooling at 5 °C per hour. X-ray diffraction analysis reveals that both types of crystals show different compositions and cell parameters. C3a_1 crystallises in a monoclinic *C2/c* space group, whereas C3a_2 crystallises in a tetragonal *P4₃22* space group. Complete crystallographic para-

meters are presented in Table 1. In both cases, metal centres, Ni(II), adopt distorted octahedral but asymmetric units and accordingly the coordination environment shows wide differences. The asymmetric unit (ORTEP) contents are presented in SI(1), which clearly indicate the presence of uncoordinated DPP molecules, a nitrate anion and two water molecules in C3a_2, as also observed in C2c, except for the nitrate anion, while all ligands are involved in the coordination sphere in C3a_1. Thus, two molecules each of DPP, bpy and water coordinate with Ni(II) in C3a_1, while the same is observed in C3a_2 with four bpy and two water molecules.

The asymmetric unit in C3a_1 has Ni1 in a twofold axis and directly bonded to O2 of a DPP ligand, to O3 of a water oxygen and to N1 of the bpy ligand, which also lies about the twofold axis. The corresponding Ni–O distance range is 2.060–2.124 Å in C3a_1 and 2.086–2.095 Å in C3a_2, respectively. Similarly, Ni–N distances are in the range of 2.086–2.095 Å for C3a_1 and the same are 2.107–2.124 Å in C3a_2 (see Table 2). The different coordination spheres present in both structures (C3a_1 and C3a_2) are shown in Fig. 12.

Furthermore, in C3a_1, the coordination spheres extend in the form of a 1D linear chain [Fig. 13(a)] through the



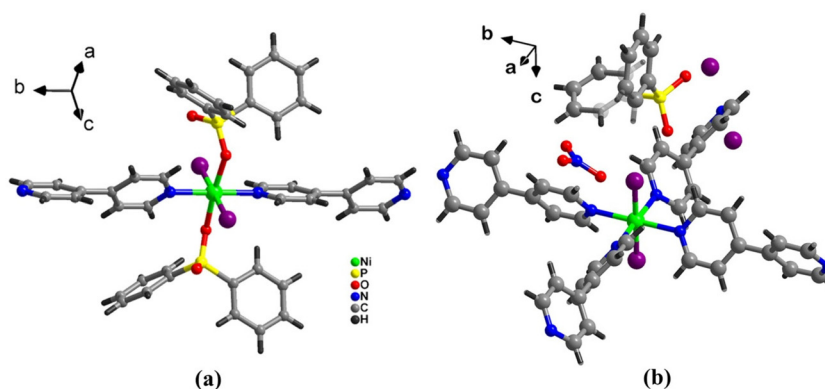


Fig. 12 View of octahedral coordination spheres of complexes (a) **C3a_1** and (b) **C3a_2**. Water molecules are shown in purple color.

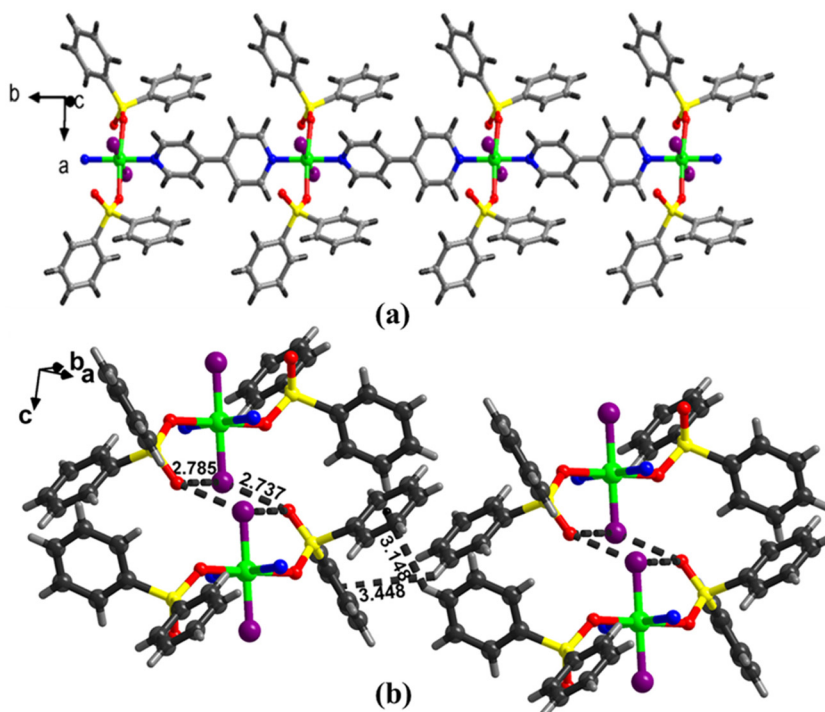


Fig. 13 (a) 1D linear chain of **C3a_1**. (b) Packing diagram of **C3a_1** showing O...O distances and C–H...O interactions.

N-terminal of bpy only. However, **DPP**, being mononucleating (Scheme 1 mode I) in this structure, is involved in the formation of strong O–H...O hydrogen bonds (O...O, 2.737(2) Å, intermolecular and 2.785(2) Å), establishing connectivity with coordinated water molecules in the adjacent chains, as well as C–H... π interactions (3.148 and 3.448 Å) between adjacent **DPP** molecules, as shown in Fig. 13, thereby effectively contributing to the stabilisation of chains and also crystal lattice.

The asymmetric unit contains Ni1 on a twofold axis coordinated to O1 (H₂O, general position) and to N1 (twofold axis) and N4 (general position) from two bpy ligands. A half nitro group (N3/O3) lies on a twofold axis. One **DPP** ligand and a second water O6 occupy general positions, and another water O7 resides on a twofold axis (half occupancy). Hydrogen

atoms attached to O6 and O7 were not modelled due to weak/ambiguous difference map density (ORTEP in the SI). Contacts involving these sites are given as O...O distances only. Crystal structure analysis of complex **C3a_2** shows that the uncoordinated **DPP** molecules remain in the crystal lattice as the structure stabilization moiety through the formation of appropriate hydrogen bonds [SI(II)] (C–H...O distances are in the range of 2.33 to 2.89 Å and O...O distances accompanying strong hydrogen bonds are in the range of 2.64 to 3.02 Å.) with further uncoordinated species nitrate and water molecules, as presented in Fig. 14. The coordinated water molecules participate in O–H...O hydrogen bonding, with O...O distances in the range of 2.63–3.67 Å. As four bpy molecules are coordinated to Ni(II) in **C3a_2**, they construct a 2D framework with a square



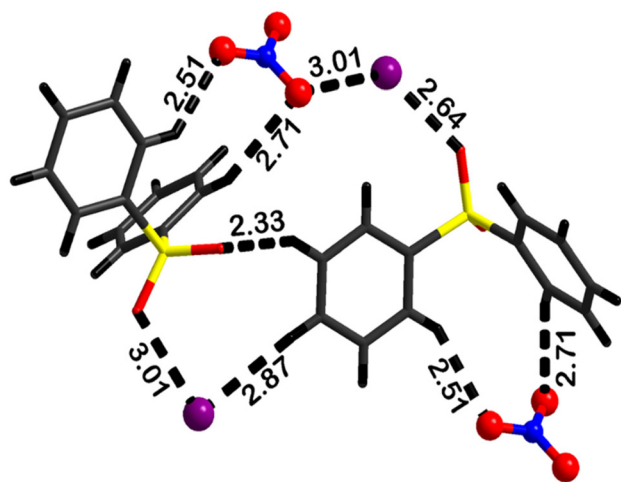


Fig. 14 Nitrate ions and uncoordinated DPP connected by H-bonds formed through uncoordinated fragments in **C3a_2**.

grid, which leads to the formation of channels along the represented axes, and the uncoordinated **DPP**, nitrate and water molecules occupy these channels, as shown in Fig. 15. The corresponding hydrogen bonds [SI(II)] between coordinated and uncoordinated fragments extend the structure through a channel like topology.

3.4. Structural elucidation of Cu(II) complexes (**C4a**, **C4b** and **C4d**)

Crystallisation experiments of $\text{Cu}(\text{ClO}_4)_2 \cdot 6\text{H}_2\text{O}$ with **DPP** in the presence of different N-heterocyclic ligands (**a–d**, as listed in Scheme 2) are carried out as mentioned in section 1.2. Three complexes, labelled **C4a** ($\text{C}_{34}\text{H}_{29}\text{ClN}_2\text{O}_9\text{P}_2\text{Cu}_2$), **C4b** ($\text{C}_{24}\text{H}_{22}\text{ClN}_2\text{O}_6\text{PCu}$) and **C4d** ($\text{C}_{24}\text{H}_{20}\text{ClN}_2\text{O}_7\text{PCu}$), with good quality mountable crystals, are formed with bpy, bpyee and 110phen, respectively. Their structural descriptions with a view of the different coordination modes of **DPP** and the counterion in the crystal lattices are given in the following paragraphs.

3.4.1. Crystals of 4a. In a controlled vacuum evaporation of a solution of **DPP** along with copper salt and bpy, the crystals obtained, **C4a**, show an asymmetric unit in a monoclinic $C2/c$ space group. It contains two copper metal ions in the asymmetric unit along with two **DPP** and one molecule each of bpy and a water molecule coordinating to them with an uncoordinated counter ion ClO_4^- , as shown in Fig. 16(a). Cu1 is bonded to O2 and O6 from two **DPP** ligands, and Cu2 is bonded to N1(bpy), O1(**DPP**), and O4 (hydroxyl group) as shown in ORTEP (see SI(II)). A perchlorate anion is present in a general position. Cu–O and Cu–N distances are in the ranges of 1.924–2.339 Å and 2.013–2.016 Å, respectively (see Table 2). The distance between two metal centres Cu1 and Cu2 is found to be 3.230 Å, and the dimeric unit forms a cage-like structure upon extension.

The cage-type moieties thus formed (made up of metal, oxygen and phosphorous atoms) further expand into the polymeric form through bridging by bpy ligands, as presented in Fig. 17. Furthermore, ClO_4^- ions contribute to the stabilization of the structure with the formation of appropriate C–H...O (H...O, 2.43–2.79 Å) hydrogen bonds with both **DPP** and bpy ligands, as depicted in the inset of Fig. 17. Hydrogen bond parameters are listed in SI(II).

3.4.2. Coordination assembly of 4b. **DPP** and bpyea, along with Cu(II), by a solvothermal crystallization process form crystals in a monoclinic $P2_1/c$ space group. The structure determination parameters are given in Table 1. In the crystal lattice, Cu(II) forms a distorted square pyramid coordinating to two bpyea, two **DPP** equatorially and ClO_4^- axially, as shown in Fig. 18. The asymmetric unit has Cu1 in a general position, directly bonded to perchlorate (O3), bpyea (N1) and **DPP** (O1). The axially placed Cu–O distance is 2.561 Å, which is comparatively larger than those known in the related structures, due to Jahn–Teller distortions, and equatorial bond distances are in the ranges of 1.929–1.934 Å for Cu–O and 1.995–2.004 Å for Cu–N (Table 2).

In this complex, **DPP** molecules follow a bidentate bridging mode, expanding the chain infinitely in the *a* direction.

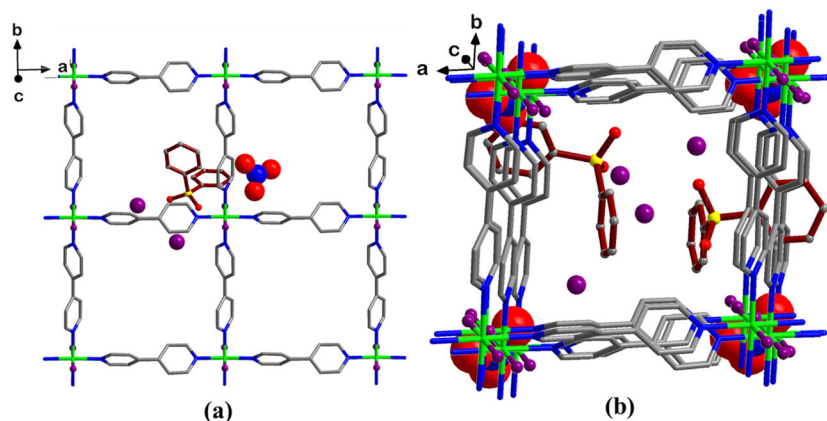


Fig. 15 (a) 2D square grid framework of **C3a_2**. (b) Channel structure of **C3a_2** showing **DPP** (maroon), nitrate (space filling) and water molecules (purple) inside the channel.



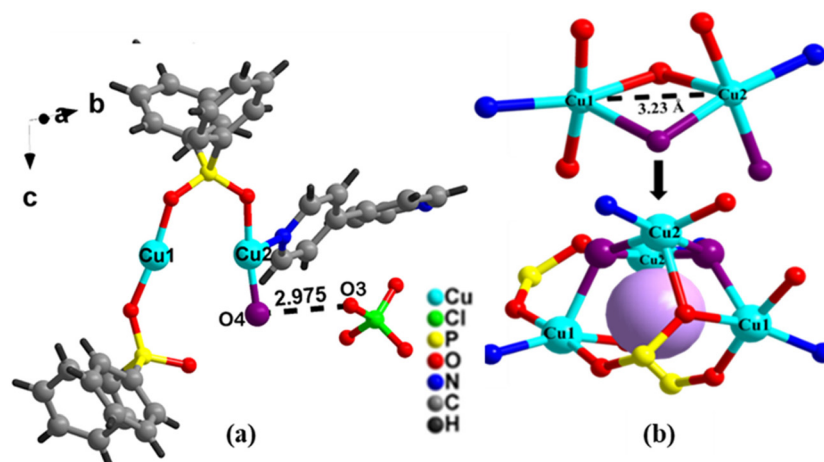


Fig. 16 (a) Representation of the asymmetric unit of **C4a** illustrating two copper metal centres. Oxygen (–OH) in purple colour with an O–O distance of 2.975 Å with ClO_4^- (b) dimeric unit with two distorted square pyramidal copper metal centres aggregated into a cage-like structure.

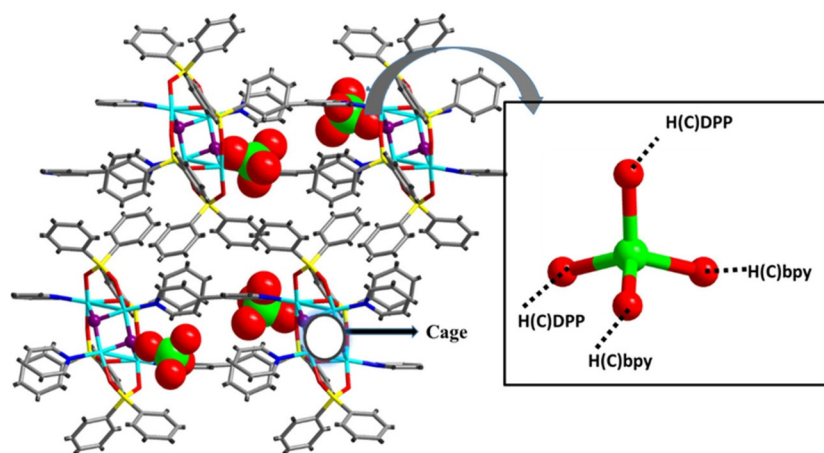


Fig. 17 Packing diagram of the cage-based framework of **C4a** encapsulating ClO_4^- . Hydrogen bonding involving ClO_4^- is illustrated in the inset.

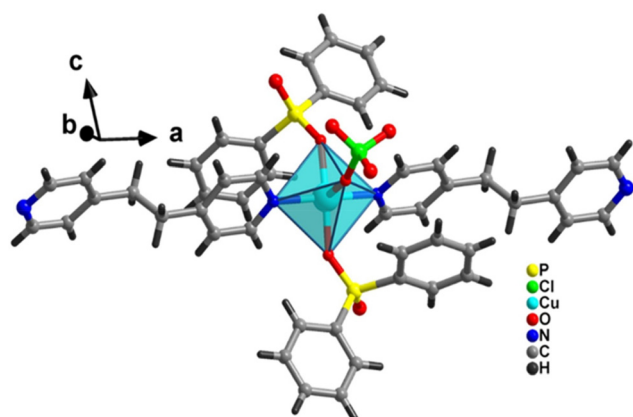


Fig. 18 View of distorted square pyramidal **C4b**.

Similarly, bpyea, coordinated with Cu(II), also contributes to the extension of the molecular arrangement in the other directions, thus leading to the formation of a 2D framework (see Fig. 19). As noted in the structure of **C4a**, herein ClO_4^- anions also contribute to the crystal stabilization by participating in the formation of C–H...O ($\text{H}\cdots\text{O}$, 2.40 and 2.41 Å) and hydrogen bonds with **DPP**, as shown in the inset of Fig. 19. Apart from this, bpyea is also involved in strong C–H...O bonds, as shown in SI(II).

3.4.3. Structure of C4d. Crystals of **C4d**, obtained from a solvothermal crystallisation method, crystallize in an orthorhombic space group *Pbca*. In the asymmetric unit, Cu(II) adopts a distorted square-pyramidal geometry, coordinated equatorially by one DPP ligand (O1), one H_2O molecule (O3), and two N donors from 1,10-phenanthroline (N1, N2); the axial site is occupied by a perchlorate O atom (O4) (Fig. 20a). In this structure, **DPP** molecules act as a monodentate ligand,



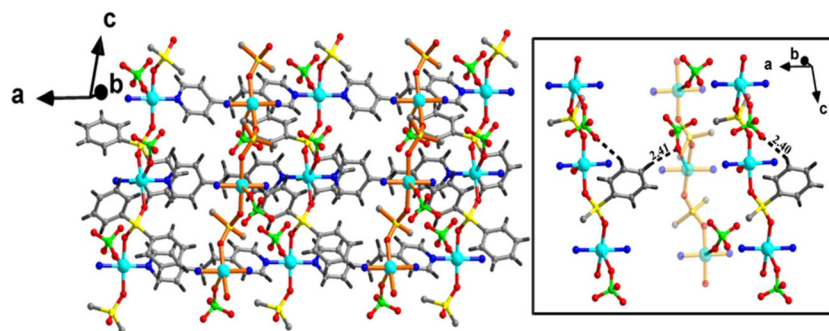


Fig. 19 2D framework of **C4b**. C–H...O is shown in the inset (for clarity purposes, phenyl rings are omitted).

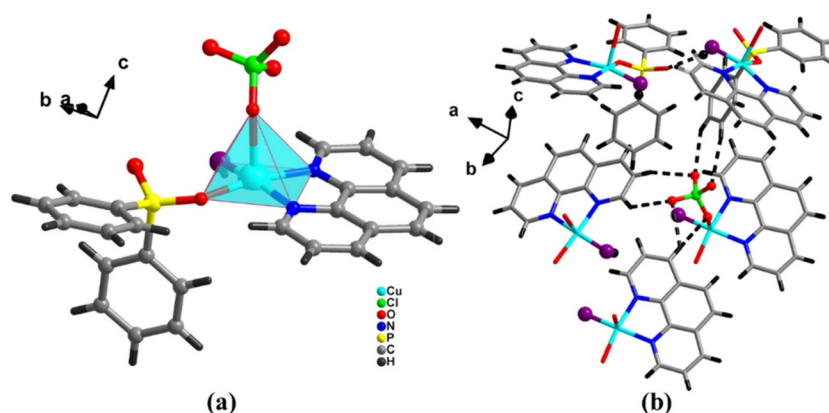


Fig. 20 (a) View of the distorted square pyramidal environment of **C4d**. (b) Non-covalent interactions between adjacent discrete molecules. Water molecules are shown as purple spheres.

resulting in discrete coordination units in complex **C4d**, unlike in **C2d**, where a bidentate mode constructs the dimeric form (cf. Fig. 10).

Fig. 20(b), however, shows the interconnection between adjacent discrete molecules *via* C–H...O (H...O, 2.33–2.83 Å) and O–H...O (H...O, 1.64 Å) hydrogen bonds, as detailed in SI(2). The two-dimensional packing arrangement of the

complex along the *a*-axis is illustrated in Fig. 21, with an inset of π – π interaction (3.52 Å) between 110phen ligands.

3.5. Structural elucidation of Cd(II) complex (C5a)

C5a ($\text{C}_{46}\text{H}_{38}\text{N}_2\text{O}_6\text{P}_3\text{Cd}$), a coordination complex of **DPP** and bpy coordinated to Cd(II), is the lone structure obtained upon crystallization of **DPP** with Cd(II) and different N-donor ligands (a–d), following a slow evaporation method at room temperature. The asymmetric unit contains Cd1 at a general position,

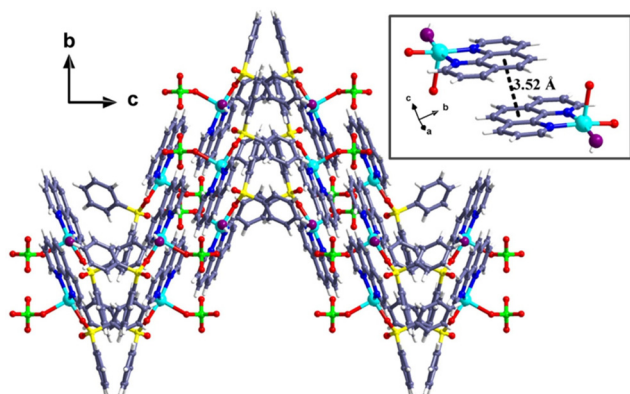


Fig. 21 Packing arrangement view of **C4d** along the *a*-axis. π – π interaction between phenanthroline ligands is shown in the inset.

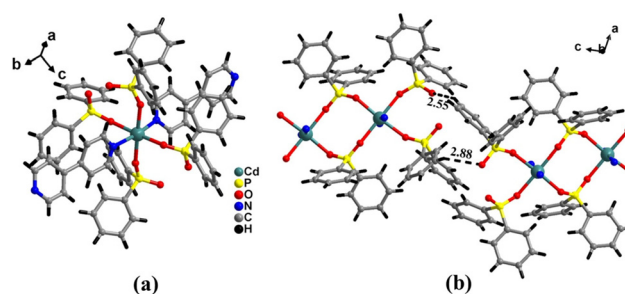


Fig. 22 (a) View of the octahedral environment of **C5a**. (b) Non-covalent interactions (C–H...O shown in Å) between adjacent dimeric fragments.



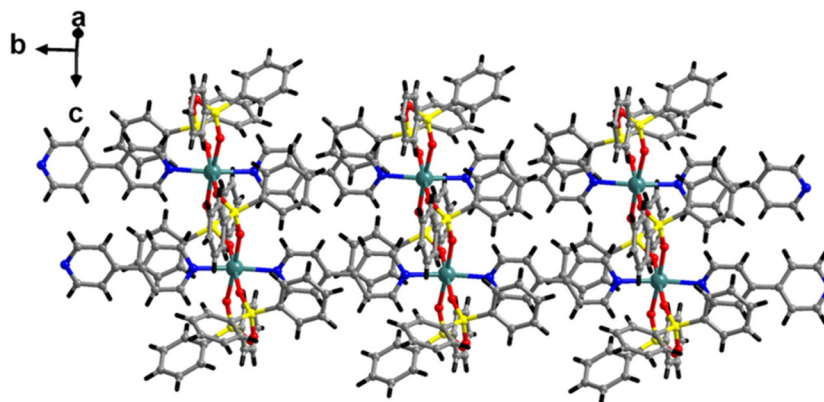


Fig. 23 2D packing arrangement of C5a illustrating polymeric chains.

directly bonded to one 4,4'-bipyridine (bpy), and three crystallographically independent DPP ligands (all in general positions). X-ray diffraction analysis confirms the monoclinic $C2/c$ space group. All the characteristic crystallographic parameters are listed in Table 1 and the contents of asymmetric units, in the form of ORTEP, are presented in section SI(1).

Packing analysis further reveals that $Cd(II)$ is octahedrally coordinated by four DPP and two bpy molecules as shown in Fig. 22(a), with typical Cd–O and Cd–N distances in the ranges of 2.250–2.276 Å and 2.365–2.377 Å, respectively (Table 2).

The packing arrangement of C5a is similar to that of C2b. Because both DPP ligands are involved in bidentate bridging, they form the eight-membered ring $M-(O-P-O)_2-M$, as well as pseudo-chelation through C–H...O hydrogen bonding (H...O, 2.55 and 2.87 Å), as projected in Fig. 22(b). In this process, water and DPP molecules in C2b and only DPP molecules in C5a are involved in pseudo-chelation. These dimeric complexes are extended through bpy molecules to form linear polymeric chains (Fig. 23).

5. Conclusion

In summary, different coordination assemblies are developed by varying the metal ions with a specific organophosphorus ligand and by varying N-donor species to form various supramolecular motifs with discrete to dimeric and polymeric structures including MOF and cage architectures. All complexes are thoroughly characterized and analysed by single crystal X-ray diffraction, unravelling diverse coordination geometries like square pyramidal and octahedral depending on central metal ions and the ligand environment. C1b is a 1D coordination polymer with dinucleating behaviour of DPP. Generally, when similar ligands are employed with the same metal ion species, isostructural/isomorphous structures are predicted, as is the case with $Co(II)$, DPP and N-donors (a–c). However, this is not the case among C2a–C2c complexes; though N-donor ligands act in a similar way, DPP's coordination modes are different. Consequently, C2a does not have any metal phosphinate

8-membered ring structure like C2b; meanwhile, in the case of C2c, a completely different host–guest topology is found, without the formation of any coordination bonds by DPP.

Mixed ligand strategies proved crucial in directing the assemblage of these architectures, particularly in the MOF structure of $Ni(II)$ complexes. Also, different reaction conditions (solvothetical and slow evaporation at room temperature) result in different types of crystals; for example, C3a_2 (tetragonal) is found to exhibit a higher symmetry lattice in comparison with C3a_1 (monoclinic). Copper complexes adopt square pyramidal geometries, yet the 2D networks of C4a and C4b differ considerably, with C4a displaying a distinctive cage structure. The use of rigid N-donors like 1,10-phenanthroline (phen) results in both dimeric (C2d) and discrete (C4d) structures, even though they show similar coordination behavior. The only $Cd(II)$ complex, C5a, displays a packing pattern analogous to C2b with alternating $M-(O-P-O)_2-M$ ring motifs. Noncovalent interactions, especially O–H...O and C–H...O hydrogen bonds and $\pi-\pi$ interactions, formed by organic ligands contribute extensively to the aggregation of the complexes. This study emphasizes the importance of mixed ligands and highlights relatively less explored phosphinates in supramolecular coordination chemistry. Their versatile coordination modes and compatibility with diverse N-donors enable the construction of structurally tunable and functionally diverse architectures, highlighting their role as flexible building blocks for both discrete and polymeric assemblies with potential applications.

Conflicts of interest

There are no conflicts to declare.

Data availability

Data supporting the findings of this study are available within the article and its electronic supplementary information files, and from publicly accessible repositories. Crystallographic data for all compounds have been deposited at the Cambridge



Crystallographic Data Centre under deposition numbers CCDC 2290893–2290903.

Supplementary information (SI) is available. Supplementary Information file includes all structural studies including ORTEP and Hydrogen bond parameter of the complexes. See DOI: <https://doi.org/10.1039/d5dt01622c>.

CCDC 2290893–2290903 contain the supplementary crystallographic data for this paper.^{30a–k}

Acknowledgements

We acknowledge IIT Bhubaneswar for infrastructure facilities and support.

References

- 1 R. Silbernagel, C. H. Martin and A. Clearfield, Zirconium (iv) phosphonate–phosphates as efficient ion-exchange materials, *Inorg. Chem.*, 2016, **55**, 1651–1656.
- 2 S. A. Ondrušová, M. Kloda, J. Rohlíček, M. Taddei, J. K. Zareba and J. Demel, Exploring the Isorecticular Continuum between Phosphonate- and Phosphinate-Based Metal–Organic Frameworks, *Inorg. Chem.*, 2022, **61**, 18990–18997.
- 3 N. Hermer and N. Stock, The new triazine-based porous copper phosphonate [Cu 3 (PPT)(H 2 O) 3]·10H 2 O, *Dalton Trans.*, 2015, **44**, 3720–3723.
- 4 M. Taddei, F. Costantino, A. Ienco, A. Comotti, P. V. Dau and S. M. Cohen, Synthesis, breathing, and gas sorption study of the first isorecticular mixed-linker phosphonate based metal–organic frameworks, *Chem. Commun.*, 2013, **49**, 1315–1317.
- 5 C.-Y. Gao, J. Ai, H.-R. Tian, D. Wu and Z.-M. Sun, An ultra-stable zirconium-phosphonate framework as bifunctional catalyst for highly active CO₂ chemical transformation, *Chem. Commun.*, 2017, **53**, 1293–1296.
- 6 X. Chen, Y. Peng, X. Han, Y. Liu, X. Lin and Y. Cui, Sixteen isostructural phosphonate metal–organic frameworks with controlled Lewis acidity and chemical stability for asymmetric catalysis, *Nat. Commun.*, 2017, **8**, 2171.
- 7 P. Salcedo-Abraira, R. Serrano-Nieto, C. Biglione, M. A. Cabrero-Antonino, S. M. Vilela, A. A. Babaryk, D. Tilve-Martínez, A. Rodríguez-Diéguez, S. Navalón, H. García and P. Horcajada, Two Cu-Based Phosphonate Metal–Organic Frameworks as Efficient Water-Splitting Photocatalysts, *Chem. Mater.*, 2023, **35**, 4211–4219.
- 8 A. D. Firmino, R. F. Mendes, D. Ananias, F. Figueira, J. P. Tome, J. Rocha and F. A. Almeida Paz, Pyrene Tetrakisphosphonate-Based Metal–Organic Framework: Structure and Photoluminescence, *Eur. J. Inorg. Chem.*, 2020, **2020**, 3565–3572.
- 9 Z.-X. Wang, L.-F. Wu, H.-P. Xiao, X.-H. Luo and M.-X. Li, Structural diversity and magnetic properties of seven coordination polymers based on the 2, 2′-phosphinico-dibenzoate ligand, *Cryst. Growth Des.*, 2016, **16**, 5184–5193.
- 10 A. Bulut, Y. Zorlu, R. Topkaya, B. Aktaş, S. Doğan, H. Kurt and G. Yücesan, Macrocyclic Cu(II)-organophosphonate building block with room temperature magnetic ordering, *Dalton Trans.*, 2015, **44**, 12526–12529.
- 11 S. J. Shearan, N. Stock, F. Emmerling, J. Demel, P. A. Wright, K. D. Demadis, M. Vassaki, F. Costantino, R. Vivani and S. Sallard, New directions in metal phosphonate and phosphinate chemistry, *Crystals*, 2019, **9**, 270.
- 12 K. J. Gagnon, H. P. Perry and A. Clearfield, Conventional and unconventional metal–organic frameworks based on phosphonate ligands: MOFs and UMOFs, *Chem. Rev.*, 2012, **112**, 1034–1054.
- 13 M. M. Ayhan, C. Bayraktar, K. B. Yu, G. Hanna, A. O. Yazaydin, Y. Zorlu and G. Yücesan, A Nanotubular Metal–Organic Framework with a Narrow Bandgap from Extended Conjugation, *Chem. – Eur. J.*, 2020, **26**, 14813–14816.
- 14 M. Kloda, S. Ondrušová, K. Lang and J. Demel, Phosphinic acids as building units in materials chemistry, *Coord. Chem. Rev.*, 2021, **433**, 213748.
- 15 I. Carson, M. R. Healy, E. D. Doidge, J. B. Love, C. A. Morrison and P. A. Tasker, Metal-binding motifs of alkyl and aryl phosphinates; versatile mono and polynucleating ligands, *Coord. Chem. Rev.*, 2017, **335**, 150–171.
- 16 E. S. Wiedner, A. M. Appel, S. Rauegi, W. J. Shaw and R. M. Bullock, Molecular Catalysts with Diphosphine Ligands Containing Pendant Amines, *Chem. Rev.*, 2022, **122**, 12427–12474.
- 17 D. S. Flett, Solvent extraction in hydrometallurgy: the role of organophosphorus extractants, *J. Organomet. Chem.*, 2005, **690**, 2426–2438.
- 18 A. M. Wilson, P. J. Bailey, P. A. Tasker, J. R. Turkington, R. A. Grant and J. B. Love, Solvent extraction: the coordination chemistry behind extractive metallurgy, *Chem. Soc. Rev.*, 2014, **43**, 123–134.
- 19 J. R. Turkington, P. J. Bailey, J. B. Love, A. M. Wilson and P. A. Tasker, Exploiting outer-sphere interactions to enhance metal recovery by solvent extraction, *Chem. Commun.*, 2013, **49**, 1891–1899.
- 20 D. Yakhvarov, E. Trofimova, O. Sinyashin, O. Kataeva, Y. Budnikova, P. Lönnecke, E. Hey-Hawkins, A. Petr, Y. Krupskaya and V. Kataev, New dinuclear nickel(II) complexes: synthesis, structure, electrochemical, and magnetic properties, *Inorg. Chem.*, 2011, **50**, 4553–4558.
- 21 J. S. Maass, M. Zeller, T. M. Breault, B. M. Bartlett, H. Sakiyama and R. L. Luck, Syntheses and Structures of Three Complexes of Formulas [L₃Co (μ₂-O₂P (Bn) 2) 3CoL′][L ′], Featuring Octahedral and Tetrahedral Cobalt(II) Geometries; Variable-Temperature Magnetic Susceptibility Measurement and Analysis on [(py) 3Co (μ₂-O₂PBn₂) 3Co (py)][ClO₄], *Inorg. Chem.*, 2012, **51**, 4903–4905.
- 22 K. K. Tanabe and S. M. Cohen, Engineering a metal–organic framework catalyst by using postsynthetic modification, *Angew. Chem., Int. Ed.*, 2009, **48**, 7424–7427.
- 23 K. W. Oliver, S. J. Rettig, R. C. Thompson, J. Trotter and S. Xia, Crystal Structure and Magnetic Behavior of Copper



- (ii) Dimethylphosphinate: A Chain Polymer Containing Triangular Trimetallic Bis (μ -dimethylphosphinato) copper (ii) Units, *Inorg. Chem.*, 1997, **36**, 2465–2468.
- 24 C. M. Barnes, D. S. Bohle, R. E. Dinnebier, S. K. Madsen and P. W. Stephens, Structural and Spectroscopic Studies of Two Phases of the Organometallic Chain Polymer $[\text{Ru}_2\{\mu_2: \mu_2: \eta^2\text{-O}_2\text{PMe}_2\}_2(\text{CO})_4]_n$, *Inorg. Chem.*, 1997, **36**, 5793–5798.
- 25 A. Renz, M. Penney, R. Feazell and K. K. Klausmeyer, X-Ray Crystal Structures of the Silver Complexes of 3-Pyridyldiphenylphosphinite and Its Hydrolysis Product, *J. Chem. Crystallogr.*, 2012, **42**, 1129–1137.
- 26 R. Nassar, B. C. Noll and K. W. Henderson, Solid-state studies of the Horner–Wittig reagent $[\{\{\text{Ph}_2\text{P}(\text{O})\}_2\text{CHLi}(\text{THF})\}_2\cdot\text{THF}]$ and its mixed-anion intermediate $[\{\{\text{Ph}_2\text{P}(\text{O})\}_2\text{CHLi}\}_4\cdot\{\text{Ph}_2\text{P}(\text{O})_2\text{Li}\}_2\cdot 8\text{C}_6\text{H}_6]$ formed by reaction with dioxygen, *Polyhedron*, 2004, **23**, 2499–2506.
- 27 V. Moodley, L. Mthethwa, M. N. Pillay, B. Omondi and W. E. van Zyl, The silver(i) coordination polymer $[\text{AgO}_2\text{PPh}_2]_n$ and unsupported Ag...Ag interactions derived from aminophosphinate and phosphinic acid, *Polyhedron*, 2015, **99**, 87–95.
- 28 A. V. Anyushin, D. A. Mainichev, N. K. Moroz, P. A. Abramov, D. Y. Naumov, M. N. Sokolov and V. P. Fedin, Cd^{2+} Complexation with $\text{P}(\text{CH}_2\text{OH})_3$, $\text{OP}(\text{CH}_2\text{OH})_3$, and $(\text{HOCH}_2)_2\text{PO}_2^-$: Coordination in Solution and Coordination Polymers, *Inorg. Chem.*, 2012, **51**, 9995–10003.
- 29 Y. Zhang, A.-Q. Jia, J.-J. Zhang, Z. Xin and Q.-F. Zhang, Construction of $\{\text{Mn}[\text{Ph}_2\text{P}(\text{O})\text{NP}(\text{O})\text{Ph}_2]_2\}$ units with mono- and bi-pyridines: Syntheses, molecular structures, and spectroscopic properties of manganese(ii) complexes with tetraphenylimidodiphosphinates, *Polyhedron*, 2018, **155**, 50–58.
- 30 (a) CCDC 2290893: Experimental Crystal Structure Determination, 2025, DOI: [10.5517/ccdc.csd.cc2gwws0](https://doi.org/10.5517/ccdc.csd.cc2gwws0); (b) CCDC 2290894: Experimental Crystal Structure Determination, 2025, DOI: [10.5517/ccdc.csd.cc2gwwt1](https://doi.org/10.5517/ccdc.csd.cc2gwwt1); (c) CCDC 2290895: Experimental Crystal Structure Determination, 2025, DOI: [10.5517/ccdc.csd.cc2gwwv2](https://doi.org/10.5517/ccdc.csd.cc2gwwv2); (d) CCDC 2290896: Experimental Crystal Structure Determination, 2025, DOI: [10.5517/ccdc.csd.cc2gwwv3](https://doi.org/10.5517/ccdc.csd.cc2gwwv3); (e) CCDC 2290897: Experimental Crystal Structure Determination, 2025, DOI: [10.5517/ccdc.csd.cc2gwwx4](https://doi.org/10.5517/ccdc.csd.cc2gwwx4); (f) CCDC 2290898: Experimental Crystal Structure Determination, 2025, DOI: [10.5517/ccdc.csd.cc2gwwy5](https://doi.org/10.5517/ccdc.csd.cc2gwwy5); (g) CCDC 2290899: Experimental Crystal Structure Determination, 2025, DOI: [10.5517/ccdc.csd.cc2gwwz6](https://doi.org/10.5517/ccdc.csd.cc2gwwz6); (h) CCDC 2290900: Experimental Crystal Structure Determination, 2025, DOI: [10.5517/ccdc.csd.cc2gww08](https://doi.org/10.5517/ccdc.csd.cc2gww08); (i) CCDC 2290901: Experimental Crystal Structure Determination, 2025, DOI: [10.5517/ccdc.csd.cc2gww19](https://doi.org/10.5517/ccdc.csd.cc2gww19); (j) CCDC 2290902: Experimental Crystal Structure Determination, 2025, DOI: [10.5517/ccdc.csd.cc2gww2b](https://doi.org/10.5517/ccdc.csd.cc2gww2b); (k) CCDC 2290903: Experimental Crystal Structure Determination, 2025, DOI: [10.5517/ccdc.csd.cc2gww3c](https://doi.org/10.5517/ccdc.csd.cc2gww3c).

